Journal of Luminescence 238 (2021) 118301

Contents lists available at ScienceDirect

Journal of Luminescence

journal homepage: www.elsevier.com/locate/jlumin

Efficient 3.5 μm mid-infrared emission in heavily Er^{3+}-doped fluoroaluminate glasses and its emission mechanism

Jiquan Zhang [a], Ruicong Wang [a], Xin Wang [a], Wenhao Li [a], Mo Liu [a], Shijie Jia [a], Lijun Wang [b], Yongqiang Ning [b], Hangyu Peng [b], Gilberto Brambilla [c], Shunbin Wang [a,*], Pengfei Wang [a,d,**]

[a] Key Lab of In-Fiber Integrated Optics of Ministry of Education of China, Harbin Engineering University, Harbin, 150001, China
[b] State Key Laboratory of Luminescence and Application, Changchun Institute of Optics, Fine Mechanics and Physics, Chinese Academy of Sciences, Changchun, 130033, China
[c] Optoelectronics Research Centre, University of Southampton, Southampton, SO17 1BJ, United Kingdom
[d] Key Laboratory of Optoelectronic Devices and Systems of Ministry of Education and Guangdong Province, College of Optoelectronic Engineering, Shenzhen University, Shenzhen, 518060, China

ARTICLE INFO

Keywords:
Fluoroaluminate glass
Mid-infrared fluorescence
Er^{3+}-doped
3.5 μm emission

ABSTRACT

Er^{3+}-doped fluoroaluminate glasses with different concentrations were prepared by using melt-quenching method. Under a 638 nm laser diode pumping, efficient 3.5 μm emission was observed in the 18 mol% Er^{3+} doped sample, which was ascribed to the Er^{3+}: $^4F_{9/2} \rightarrow {}^4I_{9/2}$ transition. The fluorescence properties such as radiative transition probability, energy level lifetime and branch ratio were predicted by the well-known Judd-Ofelt theory, while the emission and absorption cross-sections were calculated using the Füchtbauer-Ladenburg and McCumber theories, respectively. Both simulated and experimental results show that Er^{3+}-doped fluoroaluminate material is a promising gain medium for 3.5 μm laser applications.

1. Introduction

In recent decades, mid-infrared (MIR) lasers have become an important research topic because of the multitude of applications of high efficiency, high brightness, good stability MIR light sources in military counter-measures [1], environmental sensing [2], spectroscopy [3], material processing [4] and biomedical applications [5]. On one hand, hydroxyl has a major absorption band at 2500-3600 cm^{-1}, meaning that the detection, analysis and processing of water-containing substances can be used in medical research, where mid-infrared light is safe for handling human tissue and cells. On the other hand, many hydrocarbons show fundamental absorption bands in the MIR range, and the spectrum region 3–4 μm is particularly useful for spectral analysis because it contains the fundamental stretching frequency of the C–H covalent bond in many chemical species. Laser sources in the MIR range are widely used to the detection of greenhouse gases, such as methane and propane, and other compounds common in industrial processes (e.g. formaldehyde [3]). In materials rich in C–H bonds, wavelength-resonant polymer processing, such as cutting, molding, and welding, is possible [4]. MIR light sources could also facilitate the analysis of trace gases in breath analysis for disease identification [6], or the development of optical countermeasure systems, due to the spectral transmittance features of atmosphere [7].

The optical material selection is a key factor for obtaining high performance light sources. As known to all, there are several kinds of glass host materials for constructing light sources including silicate, tellurite, fluoride, chalcogenide, and phosphate, just to name a few. The host material phonon energy is important for mid-infrared luminescence efficiency because high phonon energies would lead to large non-radiative transition probability and thus a decrease in the radiative efficiency. Fluoride glasses have relative low phonon energy (about 580 cm^{-1}), compared with other materials such as tellurite (about 750 cm^{-1}), germanate (about 900 cm^{-1}), borate (about 1400 cm^{-1}), phosphate (about 1200 cm^{-1}) and silicate glasses (about 1100 cm^{-1}) [8]. Among fluoride glasses, fluorozirconate have been widely studied: ZBLAN material (ZrF_4–BaF_2–LaF_3–AlF_3–NaF) is relatively stable, has a wide transmission window as well as low phonon energy, thus was used in various lasing devices.

In the past few years, 3.5 μm fiber lasers have been widely investigated, greatly expanding the laser wavelength range coverage [9–20].

* Corresponding author.
** Corresponding author.
E-mail addresses: shunbinwang@hrbeu.edu.cn (S. Wang), pengfei.wang@tudublin.ie (P. Wang).

https://doi.org/10.1016/j.jlumin.2021.118301
Received 28 August 2020; Received in revised form 17 June 2021; Accepted 22 June 2021
Available online 2 July 2021

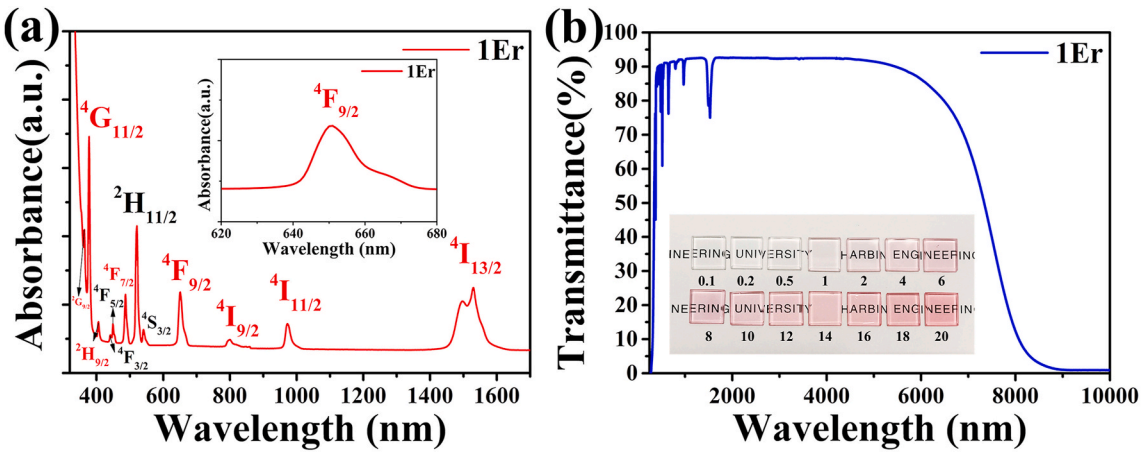

Fig. 1. (a) Absorption spectrum (320–1700 nm) of the 1 mol% Er^{3+}-doped fluoroaluminate glass sample. Inset: An enlargement of the pump band. (b) Transmittance spectrum (250–10000 nm) of the 1 mol% Er^{3+}-doped fluoroaluminate glass sample. Inset: A photograph of the various fluoroaluminate glass samples with their Er^{3+} concentration noted in bold.

Since the first demonstration of a ~3.5 μm fiber laser in 1992 [9], research on ~3.5 μm lasing proceeded slowly until 2014, when Henderson-Sapir et al. increased the 3.5 μm laser output power to 260 mW in a 1 mol% Er^{3+}-doped ZBLAN fiber by using a 976 and 1976 nm dual-wavelength pumping [10]. In 2016, by using a fiber Bragg grating (FBG) as a feedback device, Fortin et al. obtained Watt-level laser output (1.52 W) at 3.44 μm in an Er^{3+}-doped ZBLAN fiber under the pump of a dual-wavelength laser (974 and 1976 nm) [11]. In the same year, Henderson-Sapir et al. reported a tunable laser with a wavelength coverage of 450 nm by using a diffraction grating as tuning element, reaching a laser output power at 3.47 μm of 1.45 W [12]. In 2017, Maes et al. wrote two FBGs with reflectivities of 90% and 30% on both ends of a 1 mol% Er^{3+}-doped ZBLAN fiber respectively, and built a monolithic integrated fiber laser cavity, increasing the power output to 5.6 W, the highest power in 3–5 μm laser output ever reported [13]. A few months later, Qin et al. demonstrated a 3.52–3.68 μm tunable laser output with a maximum output power of 0.85 W and a slope efficiency of 25.14% [14].

Although fluorozirconate glasses have significant advantages compared with other materials, their poor resistances to deliquescence limit their further development in real applications: water molecules in air greatly damage the fluorozirconate glass surface, and long-term stability in practical applications require fluorozirconate fibers to be coated on the end facet or welded to a section of a different, stable fiber. Fluorotellurite [21], fluorogermanate [22], fluorophosphate [23] and fluorogallate glasses [24] have been used for MIR luminescence. However, at present, these materials have not achieved MIR lasing due to their relatively high phonon energies and poor transmission spectra.

Fluoroaluminate glass is a fluoride material with good chemical stability and its resistance to deliquescence has been proved [25] in our previous reports. Ho^{3+}/Pr^{3+} co-doped fluoroaluminate glass fibers were used to demonstrate a 2.86 μm lasing with 173 mW in a 19 cm long home-made fluoroaluminate glass fiber [26], showing that fluoroaluminate glass has the potential to become one of the best gain materials for mid-infrared laser applications.

In this letter, we report a broad 3.5 μm MIR fluorescence in Er^{3+}-doped fluoroaluminate glasses and study its emission properties and its suitability for lasing.

2. Experiments

The Er^{3+}-doped fluoroaluminate glasses were fabricated by using melt-quenching method. The glasses molar composition was $30AlF_3$–$15BaF_2$-(20-x)YF_3–$25PbF_2$–$10MgF_2$-xErF_3 (x = 0.1, 0.2, 0.5, 1, 2, 4, 6, 8, 10, 12, 14, 16, 18, 20). After weighing, grinding and mixing, batches of the dry, high-purity (99.99%) raw materials were packed in platinum crucibles and melted in a furnace at 930 °C for 60 min in a nitrogen-atmosphere glove box. The molten liquids were then poured onto a 380 °C copper mold which was preheated, then annealed for 3 h and cooled down very slowly to 25 °C. The fluoroaluminate glass samples were polished to optical quality, the thickness is 1.85 mm ± 0.01 mm for the following optical measurements. The absorption and transmission spectra in the range of 250–2500 nm and 2500–10000 nm were collected by using a PerkinElmer Lambda 750 spectrophotometer and a PerkinElmer FT-IR Spectrometer Frontier, respectively. Fluorescence emission spectra were detected by a Zolix Omni-λ300i fluorescence

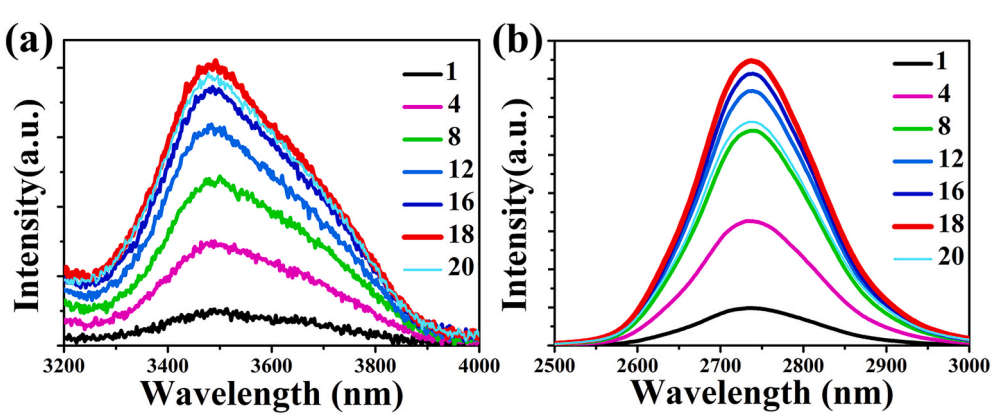

Fig. 2. (a) 3.5 μm and (b) 2.7 μm emission spectra of Er^{3+}-doped fluoroaluminate glasses.

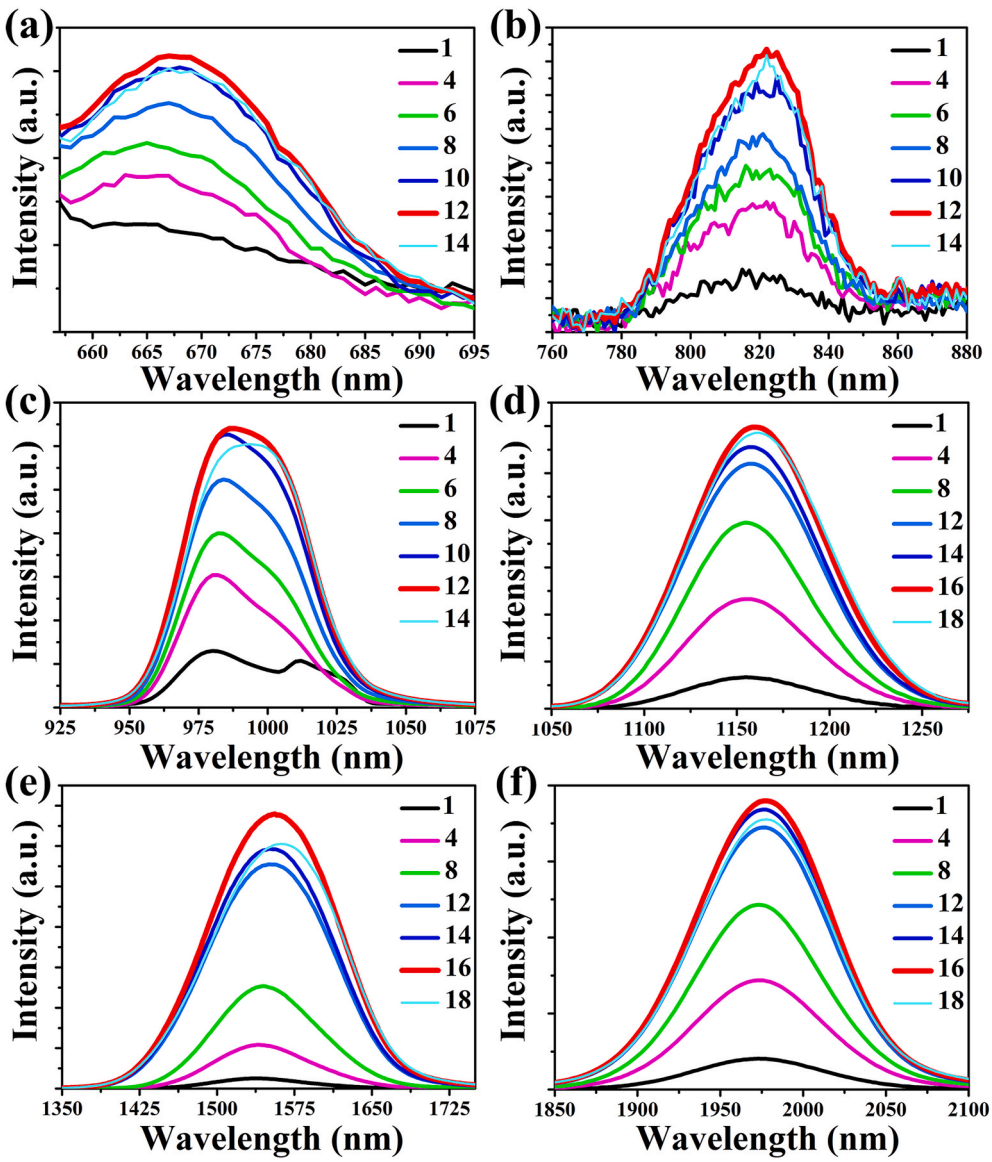

Fig. 3. (a) 670 nm ($^4F_{9/2} \rightarrow {}^4I_{15/2}$), (b) 820 nm ($^4I_{9/2} \rightarrow {}^4I_{15/2}$), (c) 990 nm ($^4I_{11/2} \rightarrow {}^4I_{15/2}$), (d) 1150 nm ($^4F_{9/2} \rightarrow {}^4I_{13/2}$), (e) 1550 nm ($^4I_{13/2} \rightarrow {}^4I_{15/2}$) and (f)1970 nm ($^4F_{9/2} \rightarrow {}^4I_{11/2}$) emission spectra in fluoroaluminate glasses with different Er^{3+} doping concentrations.

spectrometer (Detectors: InSb detector cooled by liquid nitrogen for >1800 nm; InGaAs detector operating at room temperature for <1800 nm) under the pump of a home-made 638 nm laser diode. Fluorescence decay curves were measured using a Techcomp FLS1000 fluorescence spectrometer and a Horizon II Optical Parametric Oscillator. All measurement processes were performed at 25 °C and glass samples were placed in the same position through a calibration process.

3. Results and discussion

Fig. 1 (a) is the absorption spectrum of the 1 mol% Er^{3+}-doped fluoroaluminate glass sample. The highlighted absorption peaks represent the transitions between the Er^{3+} ground state and its 12 excited states, including $^2G_{9/2}$, $^4G_{11/2}$, $^2H_{9/2}$, $^4F_{3/2}$, $^4F_{5/2}$, $^4F_{7/2}$, $^2H_{11/2}$, $^4S_{3/2}$, $^4F_{9/2}$, $^4I_{9/2}$, $^4I_{11/2}$ and $^4I_{13/2}$. Its luminescence at 3.5 μm requires the population of the $^4F_{9/2}$ energy level (3.5 μm: $^4F_{9/2} \rightarrow {}^4I_{9/2}$): the inset shows that a 638 nm is the wavelength near the absorption peak and can be used as pump for the Er^{3+} ions which can also avoid covering the emission spectra at λ~670 nm.

Fig. 1 (b) shows that the highest transmittance of the fluoroaluminate glass is ~92% with a wide transmission up to 9 μm, much better than that of germanates (~84% with cutoff wavelength at 5.8 μm) [27] or tellurides (~80%, 6.5 μm) [28,29]. Silicate materials have a major drawback for operating in the MIR: their transmittances start decreasing at around 3 μm. For these reasons, fluoroaluminate glass is a good host for developing MIR light sources. The inset of Fig. 1(b) exhibits Er^{3+} doped glass samples with the same size of 9 mm × 9 mm × 1.85 mm.

Due to the excellent transmission window of ZBLAN in the MIR and its low phonon energy, Er^{3+} luminescence in ZBLAN has been widely studied with laser applications at ~3.5 and ~2.7 μm [16,30,31]. However, only rare earth ion concentrations smaller than 10 mol% could be achieved in ZBLAN and 8 mol% in fluoroindate glass, limiting the pumping efficiency and output power level. Fig. 2 (a) and (b) show the MIR emission spectra at 3488 nm and 2736 nm, respectively, when pumped by a 638 nm laser diode at 1.0 W with a beam waist of 2 mm. For increasing Er^{3+} concentrations, the luminescence intensities at 3488 and 2736 nm increase gradually and reach a maximum at 18 mol% Er^{3+}, as shown in Fig. 2. The concentration at which quenching occurs is shown in the figure with a thin solid line.

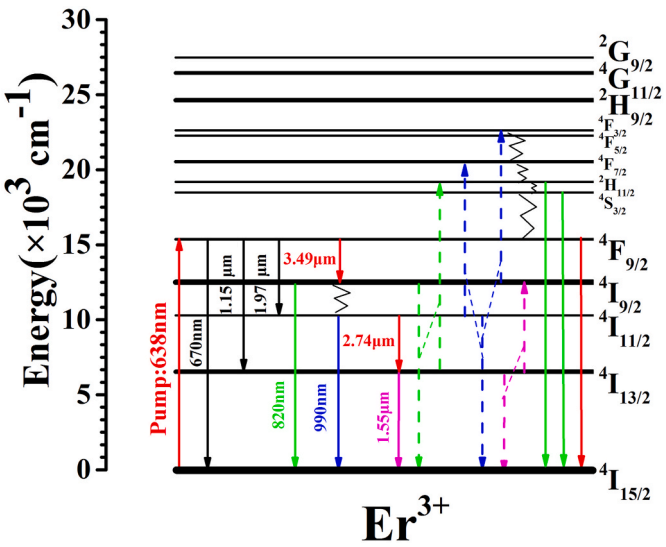

Fig. 4. Energy transfer mechanisms of Er^{3+} in fluoroaluminate glass.

To further investigate Er^{3+} luminescence in fluoroaluminate glasses, the fluorescence spectra of this material at 670 nm, 820 nm, 990 nm, 1150 nm, 1550 nm and 1970 nm have been recorded, as shown in Fig. 3. The concentrations at which quenching occurs are represented by thin solid lines. The 670 nm luminescence is observed at relatively low pump powers (0.2 W), and its efficiency (I_{670}/I_{638}) decreases for increasing 638 nm pump powers. The emission at 820 nm is very weak at high (1 W) pump powers, because the population of the $^4I_{9/2}$ energy level mainly transfers to the $^4I_{11/2}$ and other energy levels in the form of non-radiative relaxation [10,12,15,21,22]. Fig. 3 shows also other fluorescence peaks at (c) 990 nm, (d) 1150 nm, (e) 1550 nm and (f) 1970 nm. With increasing Er^{3+} doping concentration, the populations of Er^{3+} at the upper energy levels increase, thus the luminescence intensities are enhanced. The quenching concentrations are 14 mol%, 18 mol%, 18 mol % and 18 mol%, respectively.

The fluorescence spectra allow to generate the luminescence mechanism of Er^{3+} in the fluoroaluminate glass, as shown in Fig. 4. Er^{3+} absorbs the 638 nm pump light to populate the $^4F_{9/2}$ level, which then depopulates with a significant fraction of ions transferring to the ground state with emission at 670 nm and to other energy levels such as $^4I_{13/2}$ and $^4I_{11/2}$, emitting light at 1150 nm and 1970 nm. As larger fractions of the population move down to other energy levels from the $^4F_{9/2}$ level, part of it transfers to the $^4I_{9/2}$ level, producing fluorescence at 3.5 μm.

The population of the $^4I_{9/2}$ energy level follows these processes:

1. Transfer directly to the ground state, leading to a weak 820 nm luminescence.
2. Transfer to the $^4I_{11/2}$ level in the form of non-radiative relaxation, and then resulting into 990 nm and 2736 nm emissions. The $^4I_{13/2}$ level is then depopulated into the ground state, providing 1550 nm light.
3. Energy transfer up-conversion (ETU): $^4I_{9/2}+^4I_{13/2} \rightarrow {}^4I_{15/2}+^2H_{11/2}$ [32].

In addition, other ETU processes such as $^4I_{11/2}+^4I_{11/2} \rightarrow {}^4I_{15/2}+^4F_{7/2}$, $^4I_{11/2}+^4I_{9/2} \rightarrow {}^4I_{15/2}+^4F_{3/2}$ make the population of lower levels reach higher levels, and then relax onto $^4F_{9/2}$, thus enhancing the emissions at 3.5 and 2.7 μm [33,34]. At the same time, the ETU process from the $^4I_{13/2}$ level ($^4I_{13/2}+^4I_{13/2} \rightarrow {}^4I_{15/2}+^4I_{9/2}$) further enhances the 2.7 μm luminescence [33].

As shown in Fig. 5, in the 1 mol% Er^{3+}-doped glass sample, the energy level lifetimes of $^4F_{9/2}$, $^4I_{11/2}$ and $^4I_{13/2}$ are 0.41 ms, 6.26 ms and 12.08 ms, respectively. The insets show the dependence of the lifetime on the Er^{3+} doping concentration: at low concentrations (less than 0.5 mol%) the energy level lifetimes increase, as the populations of the $^4F_{9/2}$, $^4I_{11/2}$ and $^4I_{13/2}$ energy levels are small. When the concentration is larger than 1 or 2 mol%, they begin to decline. While the decline rate of the $^4F_{9/2}$ level lifetime is sudden and then stabilizes, that of $^4I_{11/2}$ is approximately linear. That is because at high Er^{3+} concentration, the spatial distance between Er^{3+} decreases, hence resonance transfer and energy transfer up-conversion between Er^{3+} ions increase significantly, leading the populations of these energy levels to decrease much faster. Simultaneously, these ETU processes depopulate lower levels to populate higher levels, increasing the emission intensities. Recycling populations to higher energy levels and emitting more photons by using ETU processes in heavily Er^{3+} doped materials, is considered to be an important technical method to improve the performance of ~3 and 3.5 μm lasers [35,36].

Four samples with 1, 8, 12 and 18 mol% Er^{3+} were used to test the fluorescence lifetimes at 3.5 and 2.7 μm. Fig. 6 (a) and (c) show the experimental lifetimes after intensity normalization. According to the fitting results, the lifetimes at 3.5 μm are 103.02, 94.05, 85.94 and 76.60 μs, while the lifetimes at 2.7 μm are 6.45, 3.96, 2.65 and 1.30 ms, respectively. The relationships between lifetimes and concentration are shown in Fig. 6 (b) and (d): as the Er^{3+} increases, the 3.5 and 2.7 μm luminescence lifetime decreases approximately linearly, reflecting the dependence of the fluorescence lifetime on the concentration.

Table 1 shows the Judd-Ofelt (J-O) parameters for the fluoroaluminate glass doped with 1 mol% Er^{3+}. The selected transitions for calculation are shown in red in Fig. 1(a). In the search of a suitable host for Er^{3+}, the magnetic dipole transitions, especially the ones involving the $^4I_{13/2}$ energy level of Er^{3+}, are not negligible. We obtained the Ω_2, Ω_4 and Ω_6 considering the Er^{3+} magnetic dipole transitions in the J-O calculation, with a mean square error Δ of 1.958×10^{-7}; the spectroscopic quality factor (Ω_4/Ω_6) is as high as 0.964, pointing to a significant benefit to achieve the desired laser transition [37].

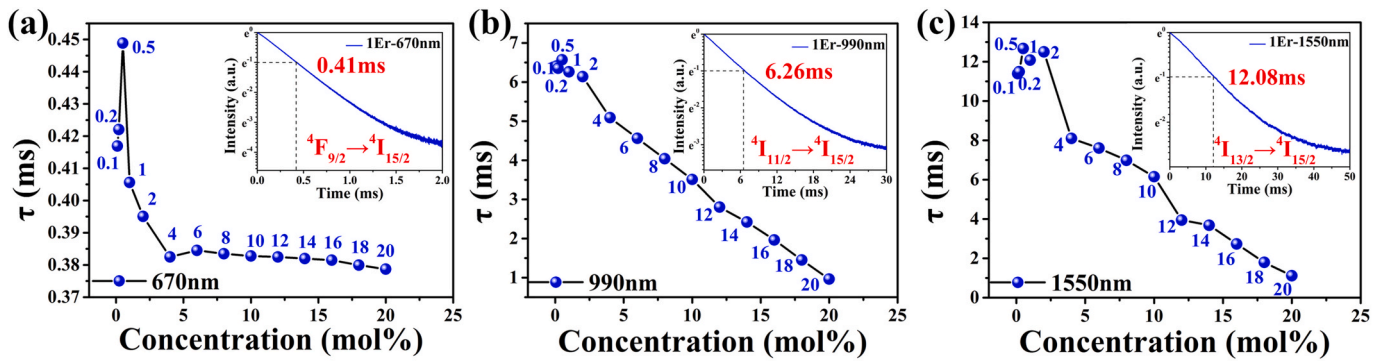

Fig. 5. Relationships between energy level lifetimes of (a) $^4F_{9/2}$, (b) $^4I_{11/2}$, (c) $^4I_{13/2}$ and the Er^{3+} doping concentration. Insets: emission decay curves in the 1 mol% Er^{3+}-doped sample.

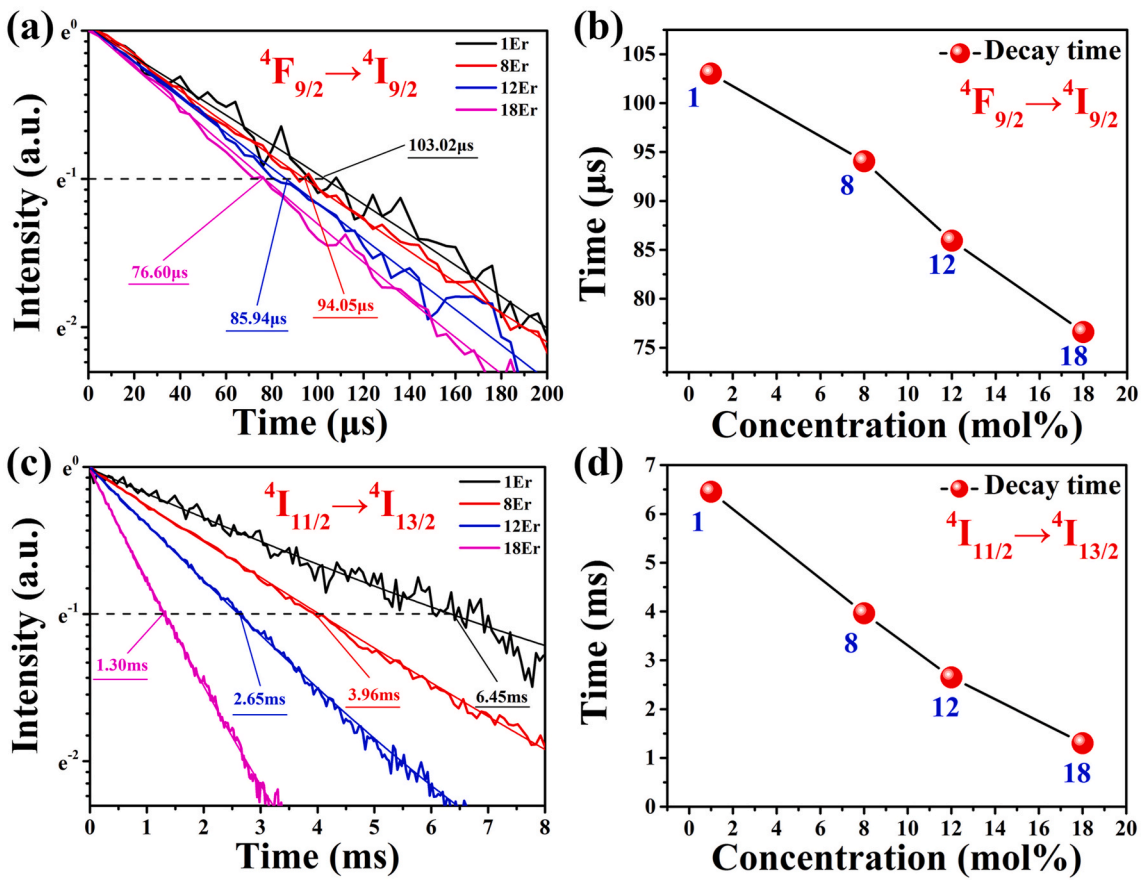

Fig. 6. (a) 3.5 and (c) 2.7 μm fluorescence lifetimes for different concentrations; smooth lines represent fit. (b) 3.5 and (d) 2.7 μm fluorescence lifetime in samples with different Er^{3+} doping concentrations.

Table 1
J-O calculated parameters for selected transitions.

SLJ	S'L'J'	EJJ'(cm^{-1})	A(ij) (s^{-1})	β(%)	τ_{rad}(ms)
$^4I_{13/2}$	$^4I_{15/2}$	6500	85.162	100.0	11.7
$^4I_{11/2}$	$^4I_{13/2}$	3600	14.289	12.3	8.6
	$^4I_{15/2}$	10100	101.502	87.7	
$^4I_{9/2}$	$^4I_{15/2}$	12250	87.404	70.0	8.0
$^4F_{9/2}$	$^4I_{9/2}$	2850	1.491	0.1	1.0
	$^4I_{11/2}$	5050	48.457	4.8	
	$^4I_{13/2}$	8650	40.724	4.0	
	$^4I_{15/2}$	15150	921.313	91.0	
$\Omega_2 = 2.021 \times 10^{-20}$ cm^2 $\Delta = 1.958 \times 10^{-7}$		$\Omega_4 = 1.194 \times 10^{-20}$ cm^2			$\Omega_6 = 1.239 \times 10^{-20}$ cm^2

Table 2
2.7 μm fluorescence lifetimes in different materials.

Material	Lifetime	Pump	Quantum Efficiency	Phonon energy	Reference
Fluoroaluminate	6.452 ms	980 nm	75.02%	615 cm^{-1}	This work
Germanate-tellurite	0.202 ms	980 nm	4.06%	650-800 cm^{-1}	[38]
Tellurite	0.215 ms	970 nm	8.26%	690 cm^{-1}	[39]
Oxysulfide	0.52 ms	980 nm	24.5%	–	[40]
Fluorotellurite	1.72 ms	980 nm	–	612 cm^{-1}	[21]

Compared with other glass materials reported in Table 2, the fluoroaluminate glass doped with 1 mol% Er^{3+} has a relatively long fluorescence lifetime at 2.7 μm with a high quantum efficiency of 75.02% ($\eta = \tau_{exp}/\tau_{rad} = 6.452$ ms/8.6 ms, much higher than that of other hosts, which is ascribed to the low phonon energy of the fluoroaluminate material. The long 2.7 μm fluorescence lifetime indicates that there is a larger fraction of the $^4I_{11/2}$ energy level population transferring to the $^4I_{13/2}$ level by means of radiative (instead of non-radiative) relaxation, improving the 2.7 μm emission efficiency.

Based on the J-O calculation results and on the 1 mol% Er^{3+}-doped fluorescence spectrum at 3.5 μm, the emission cross-section of the 3.5 μm fluorescence in the 1 mol% Er^{3+}-doped fluoroaluminate glass was calculated using the Füchtbauer-Ladenburg formula:

$$\sigma_{emi}(\lambda) = \frac{\lambda_p^4 A_{rad}}{8\pi c n^2} \cdot \frac{\lambda I(\lambda)}{\int \lambda I(\lambda) d\lambda} \quad (1)$$

where λ_p is the central wavelength of the fluorescence spectra, A_{rad} is the spontaneous transition probability, c, n are the speed of light and the refractive index, $I(\lambda)$ is the emission intensity. According to the calculated emission cross section and the McCumber theory, the absorption cross section could be calculated by:

$$\sigma_{abs}(\lambda) = \frac{Z_{up}}{Z_{low}} \sigma_{emi}(\lambda) \exp\left[\frac{hc}{kT}\left(\frac{1}{\lambda} - \frac{1}{\lambda_p}\right)\right] \quad (2)$$

where Z_{low} and Z_{up} represent the partition functions of the lower and upper energy levels, respectively, h, k and T are the Planck constant, the Boltzmann constant, and the temperature. Fig. 7(a) shows that $\sigma_{abs} = 3.865 \times 10^{-22}$ cm^2, $\sigma_{emi} = 3.830 \times 10^{-22}$ cm^2. The gain coefficient can be calculated by the equation:

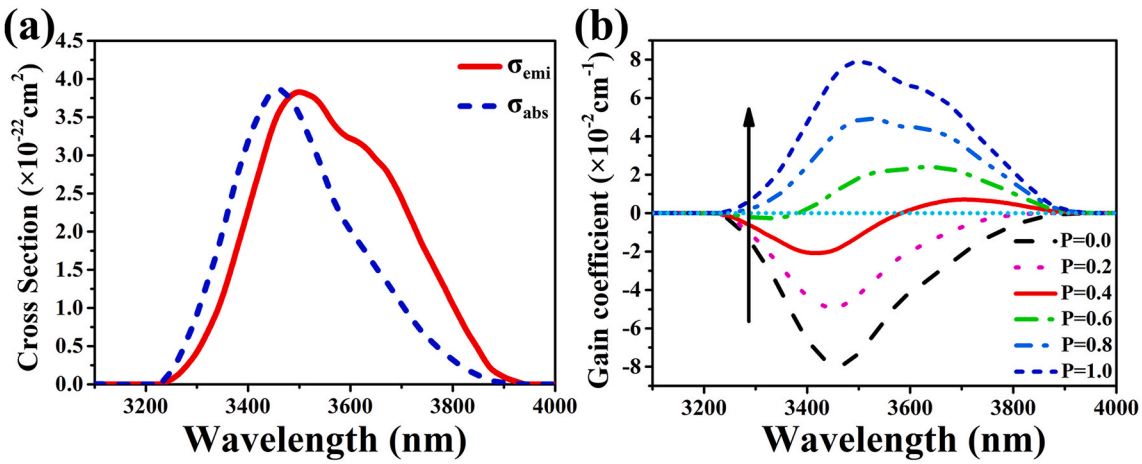

Fig. 7. (a) Calculated emission and absorption cross sections of $^4F_{9/2} \rightarrow {}^4I_{9/2}$ in the 1 mol% Er^{3+}-doped fluoroaluminate glass and (b) gain spectra based on σ_{abs} and σ_{emi} for different P values.

$$G(P) = N[P\sigma_{emi}(\lambda) - (1-P)\sigma_{abs}(\lambda)] \quad (3)$$

where N is the Er^{3+} doping concentration, and P=(the population of the upper energy levels)/(the population of total energy levels). Fig. 7(b) shows the gain spectra, calculated from 0 to 1 in steps of 0.2: a positive gain can be achieved when $P \geq 0.4$.

4. Conclusion

In summary, fluoroaluminate glasses with Er^{3+} doping concentrations from 0.1 to 20 mol% were manufactured. Absorption and transmission spectra were obtained and suitable 638 nm pump was used in the experiment to observe intense mid-infrared emissions at 3.5 and 2.7 μm. Other emission bands were also obtained, generating luminescence in Er^{3+} doped fluoroaluminate glass samples. Energy level lifetime and luminescence lifetime test results show that they have a functional relationship with Er^{3+} doping concentration. Especially, 3.5 and 2.7 μm lifetimes are on the microsecond and millisecond level. The J-O parameters, emission and absorption cross-sections of the $^4F_{9/2} \rightarrow {}^4I_{9/2}$ transition were calculated, and show that a positive gain can be achieved when P value is equal or greater than 0.4, confirming that Er^{3+}-doped fluoroaluminate glass has a great potential as a gain material to realize 3.5 μm laser sources.

Prime novelty statement

In this work, Er^{3+}-doped fluoroaluminate glasses with different concentrations were prepared by using melt-quenching method. Excellent transmission window and transmittance show the same advantages as fluorozirconate materials. Fluoroaluminate material with high doping concentration provides basis for 3.5 μm emission which was observed in this work. Other emissions at 670, 820, 990, 1150, 1550, 1970 nm and 2.7 μm were observed as well. The J-O parameters, emission and absorption cross-sections and gain spectra in 1 mol% Er^{3+}-doped fluoroaluminate glass were calculated.

Declaration of competing interest

The authors declare that they have no known competing financial interests or personal relationships that could have appeared to influence the work reported in this paper.

Acknowledgement

This work was financial supported by National Key program of Natural Science Foundation of China (NSFC61935006); National Natural Science Foundation of China (NSFC61905048, NSFC61805074); The Fundamental Research Funds for the Central Universities (HEUCFG201841, GK2250260018, 3072019CFQ2503, 3072019CF2504, 3072019CF2506, 3072020CFJ2507, 3072020CFQ2501, 3072020CFQ2502, 3072020CFQ2503, 3072020CFQ2504); The 111 project to the Harbin Engineering University (B13015); Heilongjiang Provincial Natural Science Foundation of China (LH2019F034); Heilongjiang Touyan Innovation Team Program.

References

[1] B. Molocher, Countermeasure Laser Development, SPIE, 2005.
[2] L. Jun, T. Qiulin, Z. Wendong, X. Chenyang, G. Tao, X. Jijun, Miniature low-power IR monitor for methane detection, Measurement 44 (2011) 823–831.
[3] F.K. Tittel, D. Richter, A. Fried, Mid-infrared laser applications in spectroscopy, in: I.T. Sorokina, K.L. Vodopyanov (Eds.), Solid-State Mid-infrared Laser Sources, Springer Berlin Heidelberg, Berlin, Heidelberg, 2003, pp. 458–529.
[4] M.A. Bubb, R.F. Haglund, Resonant Infrared Pulsed Laser Ablation and Deposition of Thin Polymer Films, John Wiley & Sons, Inc., 2006.
[5] Irina Sorokina, Konstantin Vodopyanov, Solid-state Mid-infrared Laser Sources, Springer, Berlin, Heidelberg, 2003.
[6] M. Mürtz, P. Hering, Online monitoring of exhaled breath using mid-infrared laser spectroscopy, E.-Z. M., S. I.T., in: Mid-Infrared Coherent Sources and Applications, Springer, Dordrecht, 2008, pp. 535–555.
[7] H.T. Bekman, J. Van Den Heuvel, F. Van Putten, R. Schleijpen, Development of a mid-infrared laser for study of infrared countermeasures techniques. Technologies for Optical Countermeasures, International Society for Optics and Photonics, 2004, pp. 27–38.
[8] W.C. Wang, B. Zhou, S.H. Xu, Z.M. Yang, Q.Y. Zhang, Recent advances in soft optical glass fiber and fiber lasers, Prog. Mater. Sci. 101 (2019) 90–171.
[9] H. Tobben, Room temperature CW fibre laser at 3.5 μm in Er^{3+}-doped ZBLAN glass, Electron. Lett. 28 (1992) 1361–1362.
[10] O. Henderson-Sapir, J. Munch, D. Ottaway, Mid-infrared fiber lasers at and beyond 3.5 μm using dual-wavelength pumping, Opt. Lett. 39 (2014) 493–496.
[11] V. Fortin, F. Maes, M. Bernier, S.T. Bah, R. Vallée, Watt-level erbium-doped all-fiber laser at 3.44 μm, Opt. Lett. 41 (2016) 559.
[12] O. Henderson-Sapir, S.D. Jackson, D.J. Ottaway, Versatile and widely tunable mid-infrared erbium doped ZBLAN fiber laser, Opt. Lett. 41 (2016) 1676.
[13] F. Maes, V. Fortin, M. Bernier, R. Vallée, 5.6 W monolithic fiber laser at 3.55 μm, Opt. Lett. 42 (2017) 2054–2057.
[14] Z. Qin, G. Xie, J. Ma, P. Yuan, L. Qian, Mid-infrared Er:ZBLAN fiber laser reaching 3.68 μm wavelength, Chin. Opt Lett. 15 (2017) 65–68.
[15] O. Henderson-Sapir, J. Munch, D.J. Ottaway, Wavelength tunable mid-infrared Er^{3+}:ZBLAN fiber laser at 3.5 μm using dual wavelength pumping, in: 2015 Conference on Lasers and Electro-Optics, CLEO), 2015, pp. 1–2.
[16] O. Henderson-Sapir, A. Malouf, N. Bawden, J. Munch, S.D. Jackson, D.J. Ottaway, Recent advances in 3.5 μm erbium-doped mid-infrared fiber lasers, IEEE J. Sel. Top. Quant. Electron. 23 (2017) 6–14.
[17] W. Höfle, H. Többen, Analysis, measurement and optimization of threshold power of 3.5 μm ZBLAN-glass fiber lasers, Int. J. Infrared Millimet. Waves 14 (1993) 1407–1424.
[18] F. Jobin, V. Fortin, F. Maes, M. Bernier, R. Vallée, Gain-switched fiber laser at 3.55 μm, Opt. Lett. 43 (2018) 1770.

[19] J. Yang, H. Zhong, S. Zhang, D. Fan, Cascade-gain-switching hybrid-pumping for generating 3.5 um nanosecond pulses from monolithic fiber lasers, IEEE Photonics Journal (2017).
[20] S.J. Jia, C.F. Yao, Z.P. Zhao, Z.X. Jia, G.S. Qin, Y. Ohishi, W.P. Qin, Flat supercontinuum generation from 1028–2804 nm in an all-solid fluorotellurite fiber, Laser Phys. Lett. 15 (2018) 115104.
[21] F. Qi, F. Huang, T. Wang, R. Ye, R. Lei, Y. Tian, J. Zhang, L. Zhang, S. Xu, Highly Er^{3+} doped fluorotellurite glass for 1.5 mum broadband amplification and 2.7 mum microchip laser applications, J. Lumin. 202 (2018) 132–135.
[22] Z. Yang, Z. Jiang, Thermal stability and spectroscopic properties of Er^{3+}-doped lead fluorogermanate glasses, J. Lumin. 121 (2006) 149–158.
[23] L. Tao, Z. Qin-Yuan, Z. Chun, F. Zhou-Ming, S. Dong-Mei, D. Zai-De, J. Zhong-Hong, Spectroscopic properties and thermal stability of Er^{3+}/Yb^{3+}-codoped fluorophosphate glasses, Chin. Phys. 14 (2005) 1250–1254.
[24] T. Xue, L. Zhang, W. Lei, M. Liao, L. Hu, Er^{3+}-doped fluorogallate glass for mid-infrared applications, Chin. Opt Lett. 13 (2015).
[25] S.J. Jia, Z.X. Jia, C.F. Yao, S.B. Wang, H.W. Jiang, L. Zhang, Y. Feng, G.S. Qin, Y. Ohishi, W.P. Qin, Ho^{3+} doped fluoroaluminate glass fibers for 2.9 μm lasing, Laser Phys. 28 (2018), 015802.
[26] S. Wang, J. Zhang, N. Xu, S. Jia, G. Brambilla, P. Wang, 2.9 μm lasing from a Ho^{3+}/Pr^{3+} co-doped AlF3-based glass fiber pumped by a 1150 nm laser, Opt. Lett. 45 (2020) 1216–1219.
[27] W.H. Dumbaugh, Infrared transmitting germanate glasses, in: Emerging Optical Materials, International Society for Optics and Photonics, 1982, pp. 80–85.
[28] K. Li, G. Wang, J. Zhang, L. Hu, Broadband 2μm emission in Tm^{3+}/Ho^{3+} co-doped TeO_2-WO_3-La_2O_3 glass, Solid State Commun. 150 (2010) 1915–1918.
[29] X. Feng, J. Shi, M. Segura, N.M. White, P. Kannan, W.H. Loh, L. Calvez, X. Zhang, L. Brilland, Halo-tellurite glass fiber with low OH content for 2-5 μm mid-infrared nonlinear applications, Opt Express 21 (2013), 18949.
[30] P. Tang, Z. Qin, J. Liu, C. Zhao, G. Xie, S. Wen, L. Qian, Watt-level passively mode-locked Er^{3+}-doped ZBLAN fiber laser at 2.8 μm, Opt. Lett. 40 (2015) 4855.
[31] Y. Shen, K. Huang, S. Zhou, K. Luan, L. Yu, A. Yi, G. Feng, X. Ye, Gain-switched 2.8μm Er^{3+}-doped double-clad ZBLAN fiber laser, in: Third International Symposium on Laser Interaction with Matter, SPIE, 2015.
[32] M. Cai, B. Zhou, F. Wang, T. Wei, T. Ying, J. Zhou, S. Xu, J. Zhang, (R = La, Y) modified erbium activated germanate glasses for mid-infrared 2.7 μm laser materials, Sci. Rep. 5 (2015) 13056.
[33] F. Maes, V. Fortin, M. Bernier, R. Vallee, Quenching of 3.4 μm dual-wavelength pumped erbium doped fiber lasers, IEEE J. Quant. Electron. 53 (2017) 1600208.
[34] Y. Lu, M. Cai, R. Cao, S. Qian, J. Zhang, Er^{3+} doped germanate-tellurite glass for mid-infrared 2.7μm fiber laser material, J. Quant. Spectrosc. Radiat. Transfer 171 (2016) 73–81.
[35] V. Fortin, M. Bernier, S.T. Bah, R. Vallée, 30 W fluoride glass all-fiber laser at 2.94 μm, Opt. Lett. 40 (2015) 2882–2885.
[36] F. Maes, C. Stihler, L.-P. Pleau, V. Fortin, J. Limpert, M. Bernier, R. Vallée, 3.42 μm lasing in heavily-erbium-doped fluoride fibers, Opt Express 27 (2019) 2170–2183.
[37] D.K. Sardar, J.B. Gruber, B. Zandi, J.A. Hutchinson, C.W. Trussell, Judd-Ofelt analysis of the $Er^{3+}(4f^{11})$ absorption intensities in phosphate glass: Er^{3+}, Yb^{3+}, J. Appl. Phys. 93 (2003) 2041–2046.
[38] Y. Lu, M. Cai, R. Cao, S. Qian, S. Xu, J. Zhang, Er^{3+} doped germanate-tellurite glass for mid-infrared 2.7μm fiber laser material, J. Quant. Spectrosc. Radiat. Transfer (2016) 73–81.
[39] L. Gomes, M. Oermann, H. Ebendorff-Heidepriem, D. Ottaway, T. Monro, A. Felipe Henriques Librantz, S.D. Jackson, Energy level decay and excited state absorption processes in erbium-doped tellurite glass, J. Appl. Phys. 110 (2011), 083111.
[40] L.D. Vila, N. Aranha, Y. Messaddeq, E.B. Stucchi, S.J.L. Ribeiro, D. Fagundes, L.A. O. Nunes, Spectroscopic properties of Er^{3+} in oxysulfide glasses, J. Alloys Compd. 344 (2002) 226–230.